Agricultural and Forest Meteorology 259 (2018) 250–259

Contents lists available at ScienceDirect

Agricultural and Forest Meteorology

journal homepage: www.elsevier.com/locate/agrformet

Multi-scale dynamics and environmental controls on net ecosystem CO_2 exchange over a temperate semiarid shrubland

Xin Jia[a,b], Tianshan Zha[a,b,*], Jinnan Gong[c], Yuqing Zhang[a,b], Bin Wu[a,b], Shugao Qin[a,b], Heli Peltola[c]

[a] Yanchi Research Station, School of Soil and Water Conservation, Beijing Forestry University, Beijing 100083, China
[b] Key Laboratory for Soil and Water Conservation, State Forestry Administration, Beijing Forestry University, Beijing 100083, China
[c] School of Forest Sciences, Faculty of Science and Forestry, University of Eastern Finland, Joensuu 80101, Finland

ARTICLE INFO

Keywords:
CO_2 flux
Eddy-covariance
Drought
Dryland
Shrub
Wavelet

ABSTRACT

Our understanding of the variability in net ecosystem CO_2 exchange (*NEE*) across different timescales is still limited, as terrestrial carbon cycle models often mismatch data at multiple timescales. Especially, multi-scale environmental controls on *NEE* are less well understood in semiarid shrublands than in mesic ecosystems. We collected eddy-covariance measurements of *NEE* over five years (2012–2016) from a semiarid shrubland in northern China, and then used continuous wavelet transform (CWT), wavelet coherence (WTC), and partial wavelet coherence (PWC) analysis to investigate how photosynthetically active radiation (*PAR*), air temperature (T_a), vapor pressure deficit (*VPD*), and soil water content (at 30-cm depth, SWC_{30}) modulate the variability of *NEE* in the time-frequency domain. CWT revealed that *NEE* not only had clear daily and annual periodicities, but also oscillated strongly at intermediate scales (days, weeks to months). At the 1-day period, *NEE* showed significant WTC with *PAR*, T_a, and *VPD* during growing seasons, with *NEE* leading *PAR* by about 1.0 h and leading T_a and *VPD* by over 3.5 h. At the 1-year period, *NEE* also showed strong WTC with *PAR*, T_a, and *VPD* throughout time, with *NEE* lagging T_a by 19 days and lagging *PAR* and *VPD* by about 40 days. At intermediate periods, non-continuous areas of significant WTC were observed between *NEE* and environmental factors, notably between *NEE* and *PAR* at 4–32-day periods during growing seasons. PWC revealed a greater modulating effect of *PAR* than that of T_a on *NEE* at intermediate periods. However, the intermediate-scale *PAR* effects were largely weakened during spring or summer drought periods (i.e., low SWC_{30}). In addition, drought events were identified as hotspots of WTC between *NEE* and SWC_{30} at monthly or longer timescales. This study highlights the need for a multi-scale approach to understanding the temporal dynamics of *NEE*. Modeling efforts should take into account these multi-temporal correlations between *NEE* and environmental factors in order to improve model-data agreement across timescales.

1. Introduction

Drylands (semiarid and arid areas) cover nearly half of the Earth's land surface (Huang et al., 2017), and they have been expanding in many regions around the world due to climate change and human activities (Berg et al., 2016; Huang et al., 2016). Recent studies highlight an important role of semiarid ecosystems in driving the global climate-carbon (C) cycle feedbacks (Poulter et al., 2014; Ahlström et al., 2015; Huang et al., 2017). Despite the importance of drylands, C exchange and its influencing factors across different timescales (i.e., hours to years) are less well understood in such ecosystems than in mesic forests and grasslands, limiting our ability to predict terrestrial C dynamics under changing climatic conditions.

Net ecosystem CO_2 exchange (*NEE*) between the atmosphere and ecosystems is simultaneously modulated by a variety of biophysical factors (e.g., radiation, temperature, precipitation, soil moisture, and vegetation) over multiple temporal scales (i.e., from seconds to years to decades) (Fig. 1). These factors exhibit a wide range of amplitudes and phases, which modulate the spectral properties of *NEE* (Stoy et al., 2005, 2009). At the hourly scale, precipitation events and changes in wind and cloud are likely to drive *NEE* dynamics through their effects on radiation, temperature, soil moisture, and stomatal conductance (Stoy et al., 2005). At the daily scale, *NEE* is driven primarily by diel cycles of solar radiation, temperature, and vapor pressure deficit (*VPD*) (Jia et al., 2014; Ouyang et al., 2014). At timescales from multi-days to multi-months, synoptic weather patterns, passages of fronts and

* Corresponding author at: Yanchi Research Station, School of Soil and Water Conservation, Beijing Forestry University, Beijing 100083, China.
E-mail address: tianshanzha@bjfu.edu.cn (T. Zha).

https://doi.org/10.1016/j.agrformet.2018.05.009
Received 10 October 2017; Received in revised form 18 March 2018; Accepted 11 May 2018

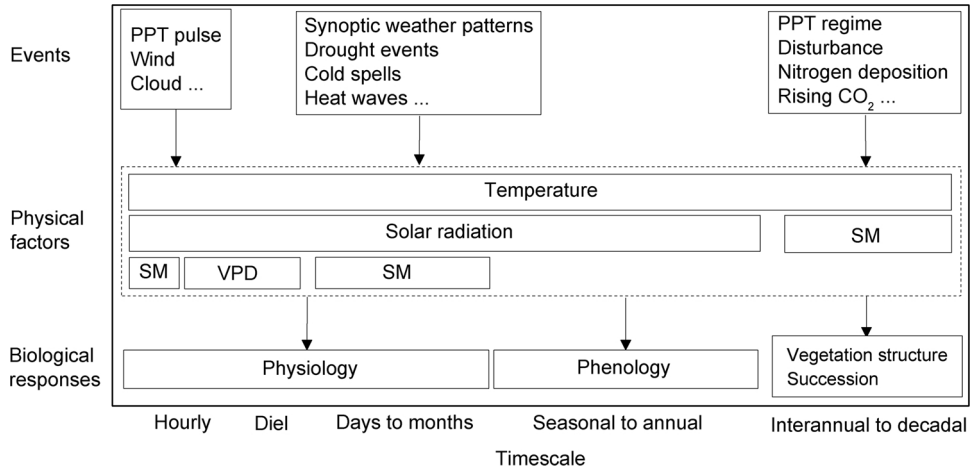

Fig. 1. A conceptual description of biophysical factors that drive net ecosystem CO_2 exchange (*NEE*) over multiple timescales. Driving factors of *NEE* included in this diagram are by no means exhaustive. Abbreviations: PPT, precipitation; SM, soil moisture; VPD, vapor pressure deficit.

pressure systems, cold spells, and heat waves can alter radiation, temperature, and water conditions, causing physiological responses and thus variations in *NEE* (Baldocchi et al., 2001; Hong and Kim, 2011). At seasonal and annual scales, *NEE* dynamics are largely affected by plant phenology and annual cycles of sunlight and temperature (Stoy et al., 2005; Ouyang et al., 2014). At interannual to decadal timescales, *NEE* may respond to climate change and variability, ecological dynamics (e.g., disturbance and succession), and environmental changes (e.g., nitrogen deposition and rising atmospheric CO_2) through changes in canopy structure or species composition (Stoy et al., 2005). Despite these understandings, process-based models rarely satisfactorily predicted *NEE* dynamics across varying timescales (Stoy et al., 2013), indicating the necessity to improve our knowledge on the variability of *NEE*. Quantifying the multi-temporal relationships between CO_2 fluxes and environmental factors is necessary for a full understanding of the climate change impacts on terrestrial C cycle (Stoy et al., 2009; Vargas et al., 2012), and could assist in the parameterization and validation of C cycle models across different timescales (Vargas et al., 2010, 2012; Stoy et al., 2013).

Current understanding on the multi-scale variability of *NEE* is mainly derived from forest ecosystems. Few studies are available on *NEE* dynamics and its controlling factors across multiple timescales in dryland ecosystems. The large uncertainty in predicting the C balance of semiarid ecosystems (Biederman et al., 2017) reflects a lack of mechanistic understanding on C dynamics across multiple timescales. Environmental controls on *NEE* in dryland areas can be different from those in mesic forests and grasslands in several ways (Jia et al., 2014, 2016a; Poulter et al., 2014). Firstly, extremely high temperature, solar radiation, and *VPD* during daytime in summer can induce partial stomatal closure, depress *NEE*, and thus shift diurnal *NEE* peaks toward morning hours (Fu et al., 2006; Jia et al., 2014). Rain pulses (and related "Birch effect") were also observed to trigger fast *NEE* responses at timescales less than a day (Huxman et al., 2004; Jarvis et al., 2007; Jia et al., 2014). Secondly, dryland ecosystems are frequently subject to droughts, wet-dry cycles, and sand storms (Huang et al., 2017), which all affect *NEE* dynamics at daily to seasonal scales. Thirdly, semiarid shrublands and steppes usually show larger seasonal and interannual variability in temperature, precipitation, and therefore in *NEE* than do mesic ecosystems (Biederman et al., 2017). Consequently, *NEE* in dryland ecosystems may have distinct spectral characteristics and multi-temporal correlations with environmental factors.

It is challenging to detect the detailed information on times, timescales, and lags of covariance between *NEE* and related environmental factors by just visually examining their time series (Baldocchi et al., 2001). Conventional analyses (e.g., correlation) suggest that biophysical controls on CO_2 fluxes vary with timescales (Fu et al., 2006; Zhang et al., 2007; Jia et al., 2014). Spectral analyses, such as Fourier or wavelet transforms, have yielded valuable insights into the temporal dynamics of *NEE* and its biophysical controls (Baldocchi et al., 2001; Qin et al., 2008; Ouyang et al., 2014). Fourier transform is well suited for stationary signals whose spectral components do not vary over time. However, CO_2 flux measurements are non-stationary in nature (Vargas et al., 2010; Ouyang et al., 2014). Moreover, scale-dependent controls on *NEE* are not constant over time, but vary within and between seasons (Cazelles et al., 2008). In contrast to Fourier transform, wavelet methods can be used to analyze transient dynamics for the association between two time series (Grinsted et al., 2004; Cazelles et al., 2008). Therefore, they are a powerful tool for exploring the variability of *NEE* and its biophysical controls. Unfortunately, few studies (if any) have applied wavelet techniques to multi-year *NEE* measurements in dryland ecosystems.

We collected half-hourly eddy-covariance (EC) measurements of *NEE* over five years (2012–2016) from a semiarid shrubland in northern China. The shrubland ecosystem lies at the south edge of the Mu Us Desert, an ecotone between semiarid and arid climates. From the mid-20th century, anthropogenic disturbances (e.g., over-grazing) have caused severe vegetation degradation in this area (Chen and Duan, 2009). Rehabilitation practices in the past two decades have promoted a dramatic expansion of shrubland distribution, which is considered a sign of desertification reversal (Jia et al., 2016b). Our previous studies have explored the diurnal, seasonal, and interannual variations of *NEE* in the shrubland ecosystem (Jia et al., 2014, 2016a). In this study we used continuous wavelet transform (CWT), wavelet coherence (WTC), and partial wavelet coherence (PWC) analysis to investigate how photosynthetically active radiation (*PAR*), air temperature (T_a), *VPD*, and soil water content modulate the variability of *NEE* (i.e., amplitudes and phases) in the time-frequency domain. We specifically addressed timescale-dependent controls and investigated whether and how their effects vary with time. We tested the hypotheses that *NEE* shows consistent daily and annual variations as influenced by cycles of solar radiation; and that *NEE* dynamics at intermediate timescales are affected by fluctuations in soil moisture, which in turn are determined by seasonal precipitation patterns.

2. Materials and methods

2.1. Study site

This study was conducted at the Yanchi Research Station (37°42′31″N, 107°13′37″E, 1530 m a.s.l.) of Beijing Forestry University.

The site is located in Ningxia, North China, with a mid-temperate semiarid continental climate. The mean annual air-temperature (1954–2014) is 8.3 °C, and the mean monthly temperatures range from −8.4 °C in January to 22.7 °C in July (data from Yanchi Meteorological Station, ~20 km from the study site). The mean annual precipitation (MAP) is 292 mm, which is much lower than the annual potential evapotranspiration (2024 mm). In addition, precipitation shows large seasonal (~80% falling during June–September) and interannual variations (145–587 mm). The soil is sandy with a bulk density of 1.54 ± 0.08 g cm^{-3}, a total porosity of 35.70 ± 3.83%, a field capacity of 20.31 ± 3.33% (g g^{-1} × 100), and a permanent wilting point of 3.64 ± 0.37% (g g^{-1} × 100) (mean ± standard deviation, n = 16) in the upper 10 cm of the soil profile. The studied shrubland is dominated by a mixture of xerophytic shrub species, including *Artemisia ordosica* (35% relative cover), *Hedysarum mongolicum* (30%), *H. scoparium*, and *Salix psammophila* (20%). A minor grass component (15% relative cover) comprises *Leymus secalinus*, *Stipa glareosa*, and *Pennisetum centrasiaticum*. The shrub canopy is about 1–1.5 m tall. Shrub roots are distributed mainly in the 20–50 cm soil layer. Soil water supply to the ecosystem depends entirely on precipitation as the groundwater table lies deeper than 8 m.

2.2. EC and supporting measurements

The EC method was used to measure *NEE* over the studied shrubland ecosystem. The EC tower has been operating since June 2011 as part of the China Terrestrial Ecosystem Research Network (CTERN) long-term flux monitoring program. The EC system, which consists of a 3D ultrasonic anemometer (CSAT-3, Campbell Scientific Inc., USA) and a closed-path fast response infrared gas analyzer (LI-7200, LI-COR Inc., USA), was mounted at a height of 6.2 m on a scaffold tower. Raw signals were recorded at 10 Hz using a data logger (LI-7550, LI-COR Inc., USA). Incident photosynthetically active radiation (*PAR*) was measured using a quantum sensor (PAR-LITE, Kipp & Zonen, The Netherlands). Air temperature (T_a) and relative humidity were measured with a thermohygrometer (HMP155 A, Vaisala, Finland). These meteorological sensors were mounted on the EC tower at 6 m above the ground. Half-hourly soil water content was measured at four depths (10, 30, 70, and 120 cm) within 20 m of the tower, with three replicate sensors (ECH_2O-5TE, Decagon Devices, USA) at each depth. We only used soil water content at 30-cm depth (SWC_{30}) in this study as our previous analyses have demonstrated that soil water at this depth was most closely related to ecosystem C, water, and energy exchange at this site (Jia et al., 2014, 2016a, b). Details on instrumentation and sampling procedures can be found in Jia et al. (2014, 2016b).

2.3. Flux calculation, quality control, and gap-filling

Half-hourly CO_2 fluxes were calculated from raw records using the EddyPro 4.0.0 software (LI-COR Inc., USA). Processing steps included spike removal, double coordinate rotation, time delay corrections, frequency response corrections, detrending (block averaging), and flux computation (Burba, 2013). The Webb-Pearman-Leuning (WPL) correction was not required because the LI-7200 outputs CO_2 and H_2O mixing ratios directly, i.e., thermal expansion and water dilution of the sampled air have already been accounted (Burba, 2013). CO_2 fluxes were despiked following Papale et al. (2006). We also screened nighttime flux values to exclude periods of insufficient turbulent mixing (friction velocity $u^* < 0.18$ m s^{-1}, Jia et al., 2016a). CO_2 fluxes passed the quality control criteria were considered acceptable as estimates of *NEE*. Downward CO_2 fluxes are indicated by negative *NEE* values (sink) and upward fluxes by positive values (source).

Instrument failure and maintenance resulted in 3, 16, 5, 1, and 7% missing CO_2 flux values for the five study years (2012–2016), respectively. The quality control procedure excluded 21–27% of annual CO_2 flux values (mostly nighttime values). Consequently, 5–18% daytime data were gap-filled to obtain complete annual time series, compared to nearly 50% during nighttime.

Small gaps (≤ 2 h) were filled using linear interpolation. A light-response function accounting for photoinhibition was used to fill larger daytime (incident $PAR \geq 5$ μmol m^{-2} s^{-1}) missing values (Jia et al., 2014, 2016a):

$$NEE_{day} = \alpha \frac{1 - \beta Q}{1 + \gamma Q}(Q - Q_c), \tag{1}$$

where NEE_{day} is daytime *NEE* (μmol CO_2 m^{-2} s^{-1}), Q is incident *PAR* (μmol photons m^{-2} s^{-1}), Q_c is the light compensation point (μmol photons m^{-2} s^{-1}); α, β, and γ are fit parameters. Seasonal variation in parameter values was taken into account by fitting Eq. (1) to consecutive windows of 500 non-missing daytime data points. To estimate missing nighttime *NEE* values (NEE_{night}), we fit an exponential function (Jia et al., 2016a) to the relationship between half-hourly NEE_{night} and soil temperature at 10-cm depth for each year. Missing values in environmental factors (PAR, T_a, VPD, and soil water content) were estimated using either complementary measurements at the site or the mean diurnal variation method (Falge et al., 2001). Detailed descriptions of flux calculation, quality control, and gap-filling procedures can be found in Jia et al. (2014, 2016a).

2.4. Data analysis

Wavelet analysis has been widely applied to the geophysical and ecological time series (Grinsted et al., 2004; Cazelles et al., 2008; Vargas et al., 2012). We here only briefly describe some basic concepts related to wavelet transform and coherence. Detailed reviews on the theory and application of wavelet analysis can be found in Torrence and Compo (1998), Grinsted et al. (2004), Cazelles et al. (2008), and Vargas et al. (2010).

The CWT of a discrete time series x_n (n = 1, …, N) sampled at a constant time interval (δ_t) is defined as the convolution integral of x_n with a scaled and translated mother wavelet, $\psi_0(\eta)$:

$$W_n^x(s) = \sqrt{\frac{\delta t}{s}} \sum_{n'=1}^{N} x_{n'} \psi_0^* \left[\frac{(n' - n)\delta t}{s} \right], \tag{2}$$

where * denotes the complex conjugate, s is the wavelet scale at which the transform is applied (Grinsted et al., 2004). We used the Morlet wavelet as it provides a good balance between the localization of time and frequency (Vargas et al., 2012; Ouyang et al., 2014). Moreover, it is a complex function (i.e., with both a real and an imaginary part), thus allowing for separate investigations of phases and amplitudes (Grinsted et al., 2004). The wavelet power spectrum (S_n) of x_n is defined as:

$$S_n(s) = |W_n^x(s)|^2. \tag{3}$$

For the relationship between two time series, namely x_n (environmental variables) and y_n (*NEE*), the cross-wavelet power spectrum (C_n), phase angle spectrum (A_n), and WTC spectrum (R_n^2) are defined, respectively, as:

$$C_n(s) = |W_n^{xy}(s)| = |W_n^x(s) W_n^{y*}(s)|, \tag{4}$$

$$A_n(s) = \tan^{-1}\left[\frac{\mathrm{Im}(W_n^{xy}(s))}{\mathrm{Re}(W_n^{xy}(s))} \right], \tag{5}$$

$$R_n^2(s) = \frac{|S(s^{-1} W_n^{xy}(s))|^2}{|S(s^{-1} W_n^x(s))|^2 |S(s^{-1}) W_n^y(s)|^2}, \tag{6}$$

where W_n^{xy} is the cross-wavelet transform, S denotes a smoothing in time and scale, $\mathrm{Im}[W_n^{xy}(s)]$ and $\mathrm{Re}[W_n^{xy}(s)]$ are the imaginary and real part of $W_n^{xy}(s)$, respectively (Terrence and Compo, 1998; Grinsted et al., 2004). A_n can be drawn as arrows in the time-frequency space for C_n or R_n^2. Arrows pointing down indicate x_n leading y_n by 90° or lagging y_n by 270°, while arrows pointing up indicate x_n lagging y_n by 90° or leading y_n by 270°. Arrows pointing left (right) indicate x_n and y_n vary anti-

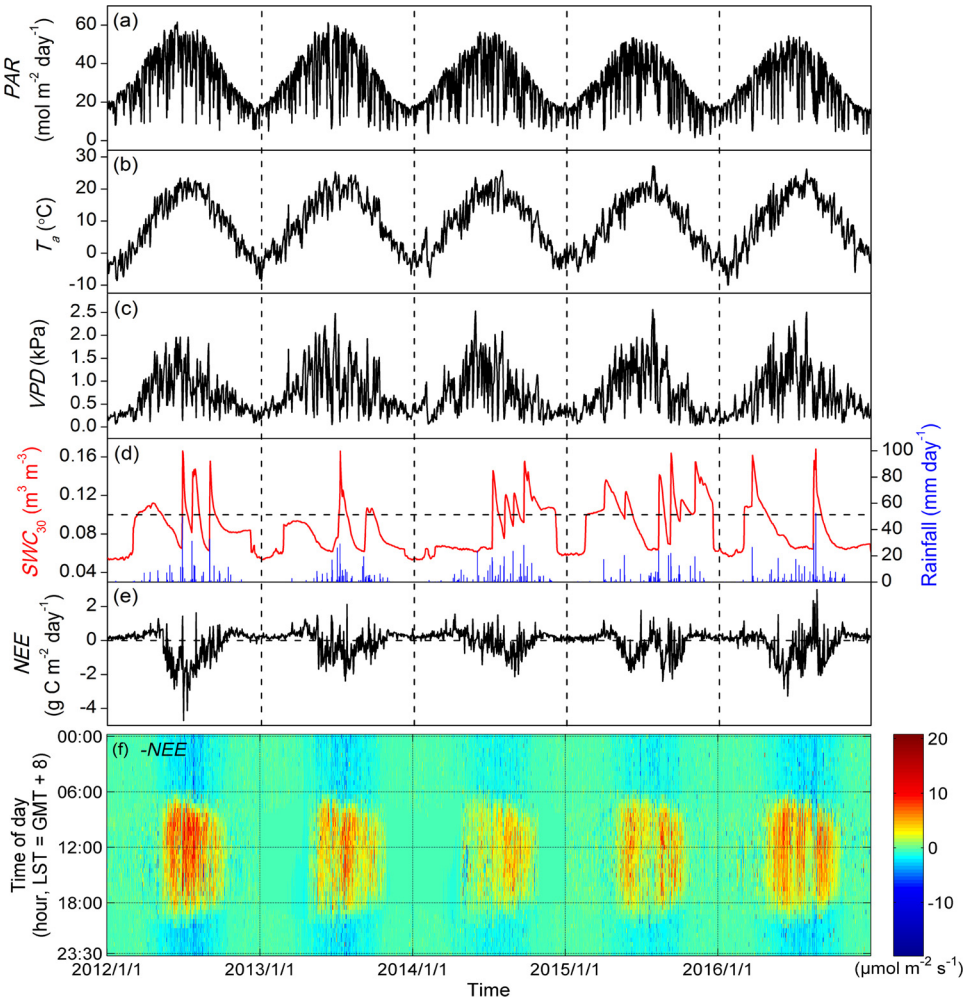

Fig. 2. Temporal variations in (a) daily-integrated incident photosynthetically active radiation (*PAR*), (b) daily mean air temperature (T_a), (c) daily mean vapor pressure deficit (*VPD*), (d) volumetric soil water content at 30-cm depth (SWC_{30}) and rainfall, (e) daily net ecosystem CO_2 exchange (*NEE*), and (f) the diurnal pattern of *NEE* for the period 2012–2016. The horizontal dashed line in (d) denotes a reference value of 0.10 m^3 m^{-3}. This reference value was identified by our previous analyses showing that both ecosystem CO_2 fluxes and sap-flow of the dominant shrub species *Artemisia ordosica* were significantly depressed when SWC_{30} was lower than 0.10 m^3 m^{-3} (Jia et al., 2014; Zha et al., 2017). More specifically, a cut point of SWC_{30} = 0.10 m^3 m^{-3} best demonstrated the differences between high and low SWC_{30} levels when analyzing the responses of *NEE* or sap-flow of *A. ordosica* to other environmental factors. The horizontal dashed line in (e) denotes the zero reference line. Vertical dashed lines separate years. Environmental factors and *NEE* values for 2012-2014 have been reported by Jia et al. (2014, 2016a, b).

phase (in-phase), respectively. However, the interpretation of phase differences should be the opposite in this study (e.g., arrows pointing left for the *NEE–PAR* relationship mean that they vary in-phase) because more negative *NEE* values indicate higher CO_2 uptake.

We also calculated the PWC spectrum (RP_n^2) (Ng and Chan, 2012) and ecosystem spectral transfer (*EST*) (Stoy et al., 2009). RP_n^2 is defined as:

$$RP_n^2(y, x_1, x_2) = \frac{|R_n(y, x_1) - R_n(y, x_2)R_n(y, x_1)^*|^2}{[1 - R_n(y, x_2)]^2[1 - R_n(x_2, x_1)]^2}, \quad (7)$$

which indicates the coherence between y_n and x_{n1} after removing the effect of x_{n2}. *EST* is defined as:

$$EST_{y,x}(s) = \log \frac{W_n^y(s)}{W_n^x(s)}, \quad (8)$$

where y_n is more (less) variable than x_n at scale s if $EST_{y,x}(s)$ is positive (negative).

The results of wavelet analysis can be presented either as local wavelet power spectra in the time-frequency domain, or as global power spectra averaged over time. A global wavelet spectrum provides information on the timescales which contribute the most to the variability of a time series, while a global cross-wavelet power spectrum (or common power) quantifies the amount of covariance that occurs between two variables across a spectrum of frequencies (Baldocchi et al., 2001; Vargas et al., 2010). WTC can be considered as a measure of local correlation between two time series in the time-frequency domain (Vargas et al., 2010; Stoy et al., 2013), while PWC is analogous to partial correlation in the time-frequency domain (Ng and Chan, 2012). The phase angle spectrum measures the time delay between two time series as a function of frequency. A statistically significant, phase-locked coherence provides a strong indication of causality (Koebsch et al., 2015). Moreover, phase angles can be used to infer causal links between processes, on the assumption that the effect must follow the cause (Vargas et al., 2010). If more than one variable showed significant coherence with *NEE* at a given timescale, we considered the variable leading *NEE* by the smallest amount of time as the primary control variable, assuming that a short response time is the best indicator of a close cause-and-effect relationship (Koebsch et al., 2015). In this study we focused mainly on WTC for examining environmental controls on *NEE*, as WTC is considered a better measure of the interrelation between two variables than cross-wavelet transform (Vargas et al., 2010). In particular, WTC can find regions in the time-frequency domain where two variables are correlated but do not necessarily have high common power (Grinsted et al., 2004).

We applied wavelet analysis to both gap-filled and non-gap-filled (zeros were padded in gaps) *NEE* time series. It turned out that gap-filling had little effect on our results (see Results and Supplementary On-line Materials). All time series were normalized before wavelet analyses to have zero mean and unit variance. The statistical significance (at 5% level) of wavelet spectra was tested using Monte Carlo methods against red noise (Grinsted et al., 2004; Vargas et al., 2010). We only presented results outside the “cone-of-influence” (COI), in which the wavelet transform suffers from edge effects due to incomplete time-locality across frequencies (Vargas et al., 2012). We performed all wavelet analyses using Matlab codes distributed by Grinsted et al. (2004) and Ng and Chan (2012).

Our previous studies at the same site identified a SWC_{30} threshold of 0.10 $m^3\ m^{-3}$, below which both ecosystem CO_2 fluxes and sap-flow of the dominant shrub species *A. ordosica* were significantly depressed (Jia et al., 2014; Zha et al., 2017). More specifically, a cut point of SWC_{30} = 0.10 $m^3\ m^{-3}$ best demonstrated the differences between high and low SWC_{30} levels when analyzing the responses of *NEE* or sap-flow of *A. ordosica* to other environmental factors. Therefore, we here used SWC_{30} = 0.10 $m^3\ m^{-3}$ as a reference value to indicate drought conditions during the growing season. This reference value is close to the stomata closure point for sandy soils (0.11 $m^3\ m^{-3}$) estimated from parameters provided in Laio et al. (2001). Using this reference point, however, does not affect our main results and conclusions.

3. Results

3.1. Variations in NEE and environmental factors in the time-frequency domain

The semiarid shrubland showed similar seasonal patterns of T_a, *PAR*, and *VPD* during the study period (2012–2016) (Fig. 2a–c). *PAR* had minimum values of less than 5 mol $m^{-2}\ day^{-1}$ in winter and maximum values of 55–60 mol $m^{-2}\ day^{-1}$ in mid-summer. Daily mean T_a ranged from about −10.0 °C in winter to 27.0 °C in summer, and daily mean *VPD* varied from low winter values of about 0.2 kPa to summer peaks of 2.0–2.5 kPa.

Seasonal variations in SWC_{30} showed clear pulse dynamics and wet-dry cycles as driven by rainfall events usually larger than 20 mm day^{-1} (Fig. 2d). The five years were characterized by contrasting seasonal patterns of SWC_{30}. Episodes of low SWC_{30} (i.e., < 0.10 $m^3\ m^{-3}$) were evident in the spring of 2014, and in the summer of 2012, 2015, and 2016. In addition, SWC_{30} was below 0.10 $m^3\ m^{-3}$ during most of the growing season in 2013, despite a pulse in mid-summer (DOY 188–207).

The five years also differed markedly in the seasonal pattern of *NEE* (Fig. 2e). Daily *NEE* varied in the ranges of −4.71 to 1.63, −2.38 to 2.13, −2.11 to 1.51, −2.41 to 1.77, −3.27 to 3.00 g C $m^{-2}\ day^{-1}$ in 2012–2016, respectively, where negative values indicate seasonal maximum strengths of C sink. By looking at time series, it is clear that changes in SWC_{30} influenced the dynamics of *NEE* (Fig. 2d–f). SWC_{30} pulses coincided with *NEE* peaks (positive), which were followed by stimulated C uptake (i.e., negative *NEE*). In contrast, drought episodes with low SWC_{30} (i.e., < 0.10 $m^3\ m^{-3}$) were characterized by remarkably depressed C sink. Multiple seasonal peaks and valleys in C uptake were observed in years (e.g., 2015 and 2016) with mid-season droughts, which caused declines in *NEE*.

As expected, the global wavelet power spectra of *PAR*, T_a, *VPD*, and *NEE* all showed strong peaks at 1-day and 1-year (365-day) periods (Fig. 3a). *PAR* also displayed strong variability (i.e., periodicity) at the 0.5-day (i.e., diurnal) period, but the power was much lower than that at the 1-day period. T_a, *VPD*, and *NEE* had smaller diurnal peaks than *PAR*. SWC_{30} showed neither daily nor diurnal spectral peak, but oscillated strongly at seasonal (i.e., around 200-day) and annual scales. In addition, these variables oscillated at intermediate (i.e., days, weeks, months) scales.

CWT clearly revealed localized features of examined variables in the time-frequency domain (Fig. 4). Except for expected diel and annual variations (Fig. 4a and b), *NEE* also oscillated at periods between 16-days and 1-year as indicated by a few bands or hotspots in the time-frequency domain. Areas of significant wavelet power for *PAR*, T_a, *VPD*, and SWC_{30} (Fig. 4c–f) corresponded to their spectral peaks in global power spectra. Notably, SWC_{30} showed non-continuous areas of significant wavelet power at intermediate periods (between 4- and 256-days).

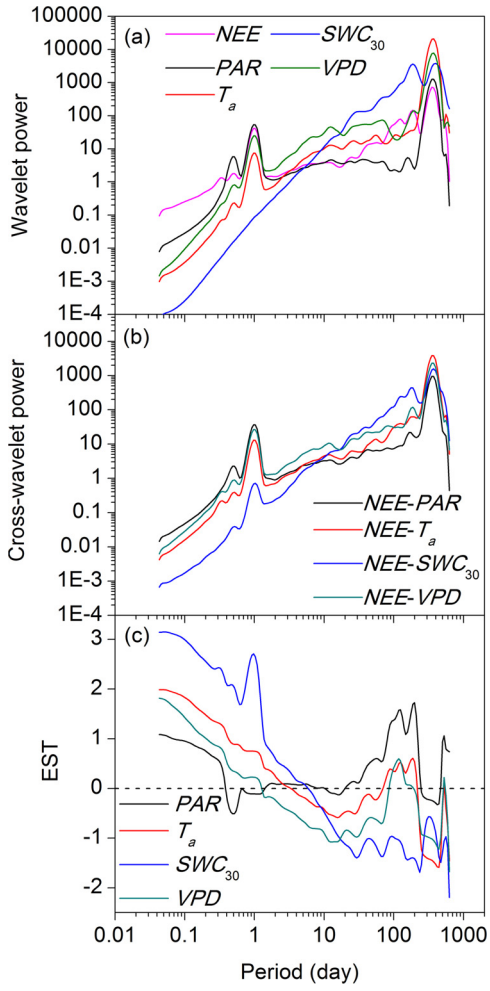

Fig. 3. Global wavelet power spectrum (a) for net ecosystem CO_2 exchange (*NEE*), soil water content at 30-cm depth (SWC_{30}), incident photosynthetically active radiation (*PAR*), vapor pressure deficit (*VPD*), and air temperature (T_a); global cross-wavelet power spectrum (b) for *NEE–PAR*, *NEE–*T_a, *NEE–SWC*, and *NEE–VPD* relationships; ecosystem spectral transfer (EST) (c) of *PAR*, T_a, SWC_{30}, and *VPD*.

3.2. Correlations between NEE and environmental factors at sub-daily to daily scales

High common power was found between *NEE* and environmental factors at daily and diurnal scales (Fig. 3b), occurring mostly during growing seasons (Figs. S1 and S2). At these scales, the variability of *NEE* was smaller than that of *PAR* (*EST* < 0), but greater than those of T_a, SWC_{30}, and *VPD* (Fig. 3c). *NEE* was more variable than all examined environmental variables (*EST* > 0) at shorter timescales (e.g., hours). At the 1-day period, *PAR*, T_a, and *VPD* were tightly correlated with *NEE* throughout growing seasons, whereas SWC_{30} showed significant WTC with *NEE* on much fewer days (Figs. 5 and S3). The phase angle between *NEE* and *PAR* was 160.82 ± 51.12° (mean ± standard deviation) at the 1-day period, i.e., *PAR* lagged *NEE* by 1.25 ± 3.32 h (Figs. 5a and 6a). In comparison, the phase angles for *NEE–*T_a and *NEE–VPD* relationships were 126.00 ± 49.56° (T_a lagging *NEE* by 3.51 ± 3.21 h) and 124.56 ± 50.09° (*VPD* lagging *NEE* by 3.60 ± 3.25 h), respectively (Figs. 5b–d, 6a). Significant PWC was hardly observed for examined relationships at sub-daily to daily scales (Figs. 7 and 8).

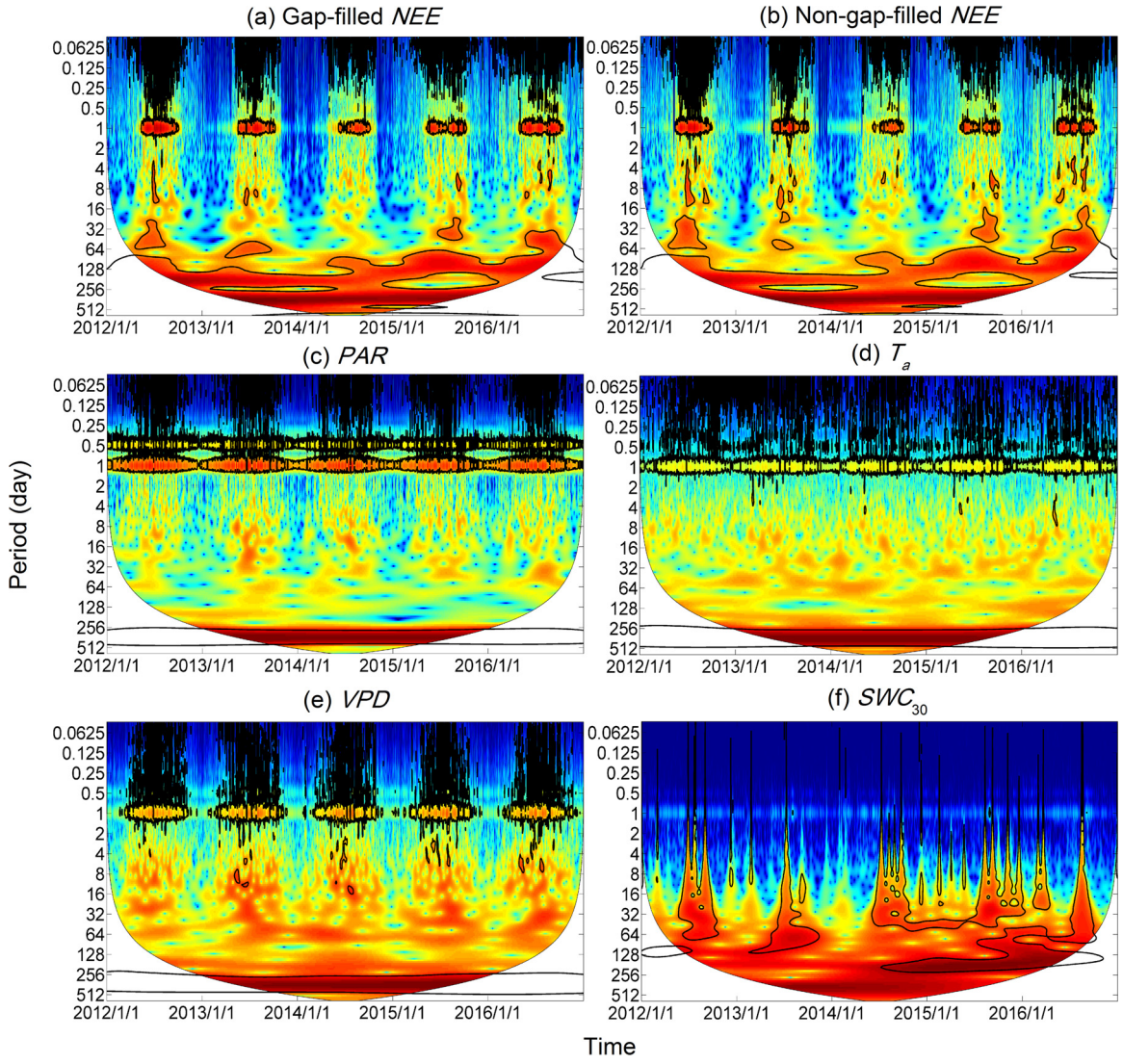

Fig. 4. Wavelet power spectrum for (a) gap-filled time series of the net ecosystem CO_2 exchange (*NEE*), (b) non-gap-filled *NEE*, (c) incident photosynthetically active radiation (*PAR*), (d) air temperature (T_a), (e) vapor pressure deficit (*VPD*), and (f) soil water content at 30-cm depth (SWC_{30}). Black contour lines represent the 0.05 significance level and the thin line indicates the cone-of-influence that delimits the region not influenced by edge effects The colour codes for power values are from dark blue (low values) to dark red (high values) (For interpretation of the references to colour in this figure legend, the reader is referred to the web version of this article).

3.3. Correlations between NEE and environmental factors at timescales of days to months

High common power was observed between *NEE* and SWC_{30} at periods from days to months (Figs. 3b, S1d, S2d). Other environmental variables showed little common power with *NEE* at intermediate scales (Figs. S1 and S2). *NEE* was generally less variable than T_a, *VPD*, and SWC_{30} ($EST < 0$) at periods between multi-days and multi-months (Fig. 3c). In comparison, *NEE* oscillated at a similar amplitude to that of *PAR* at multi-day periods, but was much more variable than *PAR* ($EST > 0$) at periods between 50- and 200-days. Non-continuous areas of significant WTC were observed between *NEE* and environmental factors over a wide range of periods (Figs. 5 and S3). These intermediate-scale WTC varied with time. Notably, significant WTC was observed between *NEE* and *PAR* during growing seasons at periods between 4- and 32-days (Figs. 5a and S3a). PWC revealed a greater modulating effect of *PAR* than that of T_a on *NEE* at intermediate periods during growing seasons (Fig. 7). However, the intermediate-scale *PAR* effects were largely weakened during spring or summer drought periods (i.e., SWC_{30} less than 0.10 $m^3\ m^{-3}$) (Figs. 5a and S3a). In addition, drought effects were identified as hotspots of WTC between *NEE* and SWC_{30} at monthly or longer timescales (Figs. 5d and S3d). The persistent drought during the growing-season of 2013 was also indicated by significant PWC between SWC_{30} and *NEE* at the bimonthly timescale (Fig. 8).

3.4. Correlations between NEE and environmental factors at the annual scale

High common power was found between *NEE* and environmental factors around the 1-year scale throughout the study period (Figs. 3b, S1, S2). At this scale, the variability of *NEE* was smaller than its influencing factors ($EST < 0$, Fig. 3c). At the 1-year period, *NEE* was tightly correlated with *PAR*, T_a, and *VPD* throughout time, but did not show consistent WTC with SWC_{30} (Figs. 5 and S3). The phase angle between *NEE* and T_a was $-161.42 \pm 6.58°$ (mean ± SD) at the 1-year period, i.e., T_a led *NEE* by about 20 ± 7 days (Figs. 5b, 6b, S3b). In comparison, the phase angles for *NEE–PAR* and *NEE–VPD* relationships were $-140.95 \pm 5.08°$ and $-141.79 \pm 7.34°$, respectively (Figs. 5a, c, S3a, c). That is, *NEE* led *PAR* and *VPD* by about 40 ± 6 days

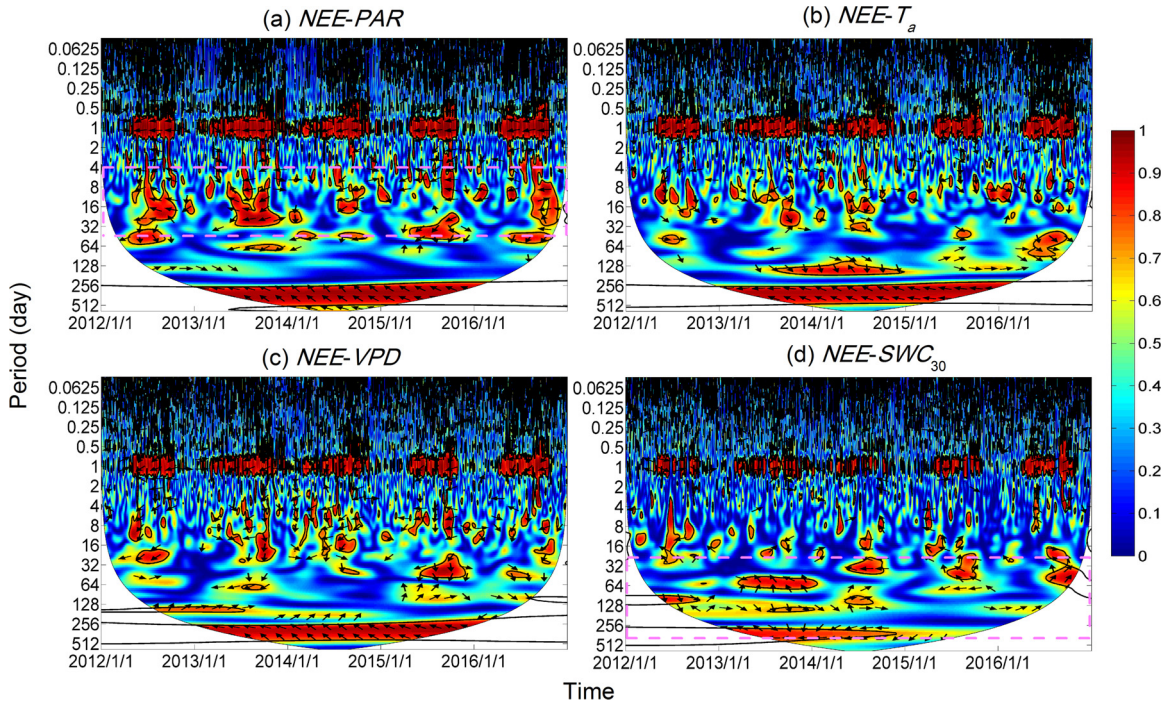

Fig. 5. Wavelet coherence between gap-filled net ecosystem CO_2 exchange (*NEE*) and (a) incident photosynthetically active radiation (*PAR*), (b) air temperature (T_a), (c) vapor pressure deficit (*VPD*), and (d) soil water content at 30-cm depth (SWC_{30}). The phase difference is shown by arrows. Arrows pointing up indicate environmental factors leading *NEE* by 90° or lagging *NEE* by 270°, while arrows pointing down indicate environmental factors lagging *NEE* by 90° or leading *NEE* by 270°. Arrows pointing left (right) indicate environmental factors and *NEE* vary in-phase (anti-phase). Black contour lines represent the 0.05 significance level and the thin line indicates the cone-of-influence that delimits the region not influenced by edge effects. The dashed rectangles in (a) and (d) indicate the frequency bands where hotspots of coherence occur.

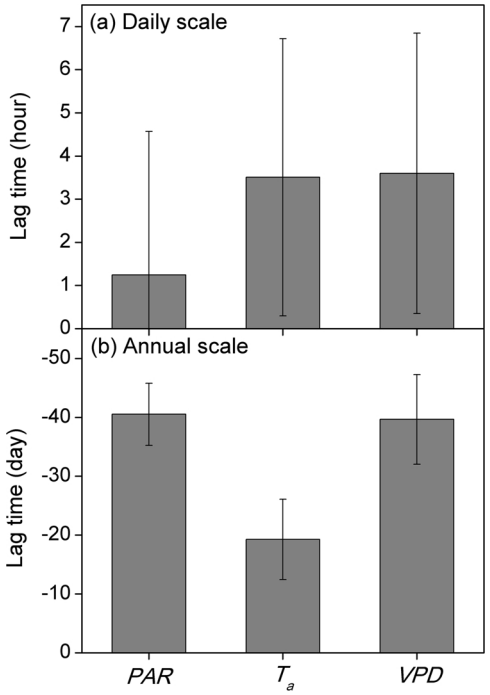

Fig. 6. Lag time between gap-filled net ecosystem CO_2 exchange (*NEE*) and environmental factors at (a) daily and (b) annual scales. *PAR*, incident photosynthetically active radiation; T_a, air temperature; *VPD*, vapor pressure deficit. Positive values indicate that *NEE* leads environmental factors, while negative values indicate the opposite. Data represent mean ± standard deviation.

(Fig. 6b). At the 1-year period, both T_a and *PAR* showed significant coherence with *NEE* after removing the effects of the other (Fig. 7). No significant PWC was found between *NEE* and SWC_{30} at the annual scale (Fig. 8).

4. Discussion

4.1. Environmental controls on NEE at daily and annual scales

Spectral peaks at daily and annual timescales are a general feature of *NEE* time series, due to the influences of solar cycles on biological activities (Baldocchi et al., 2001; Stoy et al., 2005; Ouyang et al., 2014). We found that *NEE* was more tightly correlated with *PAR* than with other environmental factors at the daily scale, as indicated by strong WTC and short lag time between *NEE* and *PAR* (1.25 ± 3.32 h) (Figs. 5, 6a, S3). C uptake is largely a function of *PAR*, while C release is usually more controlled by temperature (Jia et al., 2014). Therefore, the greater importance of *PAR* at the daily scale suggests that it was photosynthesis, rather than respiration, dominates the diel variations in *NEE* (Ouyang et al., 2014). In line with our results, Hong and Kim (2011) found that in a temperate deciduous forest the CWT spectrum for *NEE* was almost the same as that for gross ecosystem production (*GEP*), indicating that processes driving *GEP* were mainly controlling *NEE*. Moreover, canopy photosynthesis, which is a function of *PAR*, may also regulate C release at the diel scale (Tang et al., 2005; Vargas et al., 2011; Han et al., 2014). For example, WTC revealed that at the 1-day period soil CO_2 production responded to *PAR* with a mean time lag of about 5 h, but led soil temperature by 3–4 h in a mixed conifer-oak forest (Vargas et al., 2010). The regulation of C release by photosynthesis can accentuate the role of *PAR* while overshadow the role of temperature in driving *NEE* at the diel scale.

The phase difference between *NEE* and *PAR* (1.25 ± 3.32 h) agrees with our previous study (Jia et al., 2014) showing that net C uptake

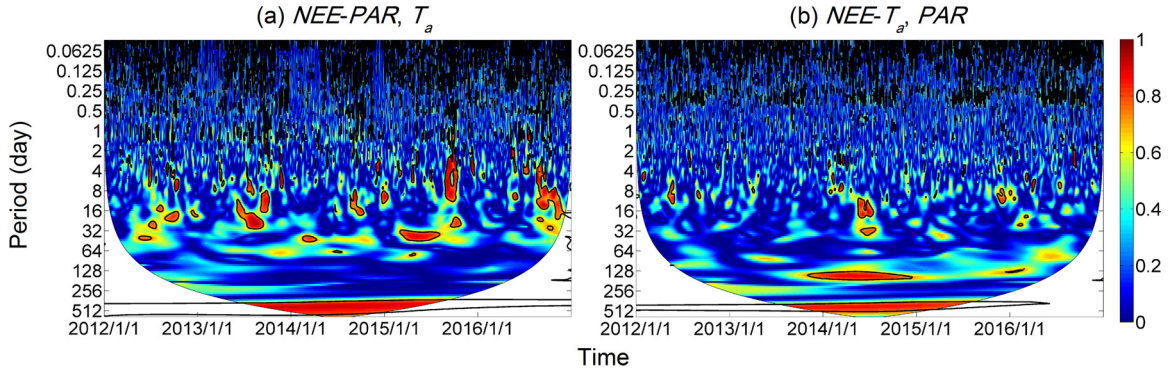

Fig. 7. Partial wavelet coherence (a) between gap-filled net ecosystem CO_2 exchange (*NEE*) and incident photosynthetically active radiation (*PAR*) after removing the effects of air temperature (T_a); and (b) between *NEE* and T_a after removing the effects of *PAR*. Black contour lines represent the 0.05 significance level and the thin line indicates the cone-of-influence that delimits the region not influenced by edge effects.

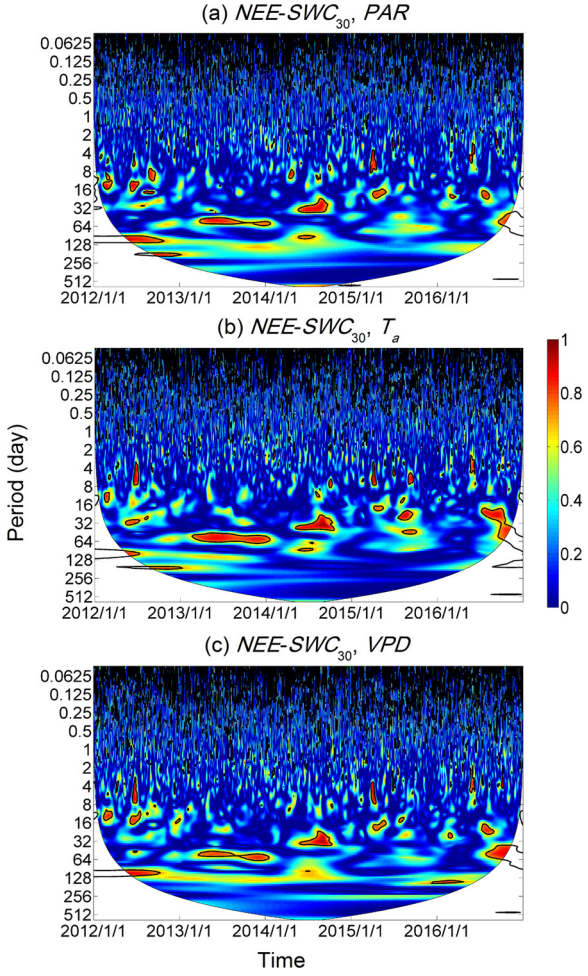

Fig. 8. Partial wavelet coherence between gap-filled net ecosystem CO_2 exchange (*NEE*) and soil water content at 30-cm depth (SWC_{30}) after removing the effects of (a) incident photosynthetically active radiation (*PAR*), (b) air temperature (T_a), and (c) vapor pressure deficit (*VPD*), one at a time. Black contour lines represent the 0.05 significance level and the thin line indicates the cone-of-influence that delimits the region not influenced by edge effects.

peaked before noon (at 9:00–10:00 LST, LST = GMT + 8) during the growing season, while *PAR* was highest between 12:30 and 13:00 LST. Many studies in arid and semiarid areas have also observed that canopy photosynthesis peaked a few hours earlier than light availability (e.g., Tang et al., 2005; Zhang et al., 2007). In water-limited ecosystems, CO_2 assimilation usually peaks at morning hours due to higher leaf water potential and photosynthetic capacity in early morning than later in the day, whereas *PAR* usually reaches maximum at noon. In addition, the diurnal asynchrony between *NEE* and *PAR* can be ascribed to mid-day and afternoon depression of net C uptake caused by high-*VPD*-induced stomatal closure and/or high-temperature-induced increases in ecosystem respiration (Jia et al., 2014). These mechanisms could also explain our result that T_a and *VPD* lagged *NEE* by ~3.5 h at the daily scale. In ecosystems with high water availability, *NEE* simply follows *PAR* on a diurnal scale. For example, WTC analysis by Ouyang et al. (2014) revealed that *NEE* oscillated in-phase with *PAR* (i.e., no time lag) at the 1-day period in an oak-dominated forest in Northwest Ohio, where MAP is 840 mm. Koebsch et al. (2015) reported a nearly in-phase diurnal relationship between *NEE* and *PAR* (a lag time of 0.2 ± 1.6 h) in a temperate wetland.

WTC and phase differences between variables revealed that *NEE* was more tightly coupled with T_a than *PAR* and *VPD* at the annual scale (Figs. 5a–c, 6b, S3a–c). This result is consistent with that found in a temperate deciduous forest (Ouyang et al. 2014). In addition, many studies have found that T_a was more important than *PAR* in controlling the spatial and temporal variations in annual CO_2 fluxes in temperate forests (Yu et al., 2013; Keenan et al., 2014). Plant phenology (e.g., leaf emergence and senescence), which influences the seasonality of *NEE*, is determined mostly by temperature instead of solar radiation (Keenan et al., 2014; Ouyang et al. 2014). We also observed earlier leaf emergence of the dominant shrub *A. ordosica* in response to warmer springs at the study site (unpublished data). In addition, temperature influences seasonal and annual variations in ecosystem respiration (Zhang et al., 2007; Jia et al., 2014, 2016a). Considering the continuing global warming trend (Huang et al., 2017), temperature may play an increasingly important role in driving plant phenology and thus *NEE* at seasonal and longer timescales. Despite the dominant role of T_a at the annual scale, both T_a and *PAR* showed significant PWC at the 1-year band throughout time (Fig. 7). In contrast, Ouyang et al. (2014) only found significant PWC for T_a, but not for *PAR*, at the same timescale. This difference suggests that solar radiation may be more important in regulating seasonal and annual C dynamics in semiarid shrublands than in temperate deciduous forests.

4.2. Environmental controls on NEE at intermediate scales

Our results are consistent with previous findings that variations in CO_2 fluxes at timescales of days to months were associated with changes in environmental factors (Baldocchi et al., 2001; Hong and Kim, 2011). For example, *NEE* has been reported to vary on synoptic timescales (i.e., days to weeks) associated with weather patterns and their effects on radiation, temperature, and moisture (Baldocchi et al., 2001; Koebsch et al., 2015). Wavelet analysis revealed monsoon-induced oscillations in *NEE* at periods of days to months in a deciduous

forest in Korea (Hong and Kim, 2011). We found that *PAR* was the primary controlling factor of *NEE* at daily to monthly timescales, especially during the growing season of 2012 and 2013, and in the late growing-season of 2014–2016 (Figs. 5a, 7a, S3a). These effects of *PAR* may be related to changes in solar radiation and thus photosynthetic activity induced by weather patterns. Our previous study at the same site (Jia et al., 2014) found that insufficient *PAR* on rainy days depressed ecosystem C uptake because of low photosynthesis rates, while excessive *PAR* on clear summer days depressed ecosystem C uptake partially due to photoinhibition of CO_2 assimilation. Similarly, Hong and Kim (2011) reported that in a temperate deciduous forest changes in net radiation during the summer monsoon season regulated *NEE* oscillations at timescales of weeks and months.

Our results showed localized impacts of soil moisture on CO_2 exchange, i.e., drought events were identified as hotspots of WTC and PWC between *NEE* and SWC_{30} at monthly or longer timescales (Figs. 5d, 8, S3d). This is in line with our previous studies demonstrating the role of seasonal water deficit in limiting canopy photosynthesis (Jia et al., 2014) and soil respiration (Wang et al., 2014) of the shrub ecosystem. Vargas et al., (2010) also found that in a semiarid mixed conifer-oak forest soil moisture and CO_2 production were significantly coherent at intermediate periods (2–32-day) as driven by discrete rain pulses. Ouyang et al. (2014) reported that drought events were responsible for *NEE* hotspots in the time-frequency domain at weekly to monthly and even longer timescales. Baldocchi et al. (2001) found that in a temperate forest the effects of summer droughts accounted for a periodicity of 10 days in the power spectrum of CO_2 fluxes. More interestingly, we also found that SWC_{30} appeared to indirectly affect *NEE* by regulating *PAR* effects at intermediate scales, i.e., WTC between *PAR* and *NEE* largely faded when the ecosystem experienced a spring or summer drought ($SWC_{30} < 0.10$ m^3 m^{-3}, Figs. 2d–f, 5a, S3a). This finding agrees with our previous analysis showing that the responses of NEE_{day} to *PAR* were markedly weakened when SWC_{30} was below 0.10 m^3 m^{-3} (Jia et al., 2014). Drought-induced stomatal closure and reductions in leaf area often depress canopy photosynthesis in semiarid ecosystems (Jia et al., 2014, 2016), obscuring *PAR* effects at timescales of days, weeks, and months. Vargas et al. (2012) also found that in a Chihuahuan Desert grassland the temporal relationship between *PAR* and soil CO_2 efflux was modified by changes in the frequency and size of rainfall events.

5. Conclusions and implications

We analyzed multi-scale dynamics and environmental controls on *NEE* over a semiarid shrubland by applying wavelet methods to a 5-year EC dataset of CO_2 fluxes. To our knowledge, this study represents the first detailed time-frequency analysis of *NEE* in semiarid shrublands. Our results indicate that multiple environmental factors may act in concert to drive *NEE* over a wide range of timescales. However, their relative importance varied with both time and timescale. *PAR* appeared to be the primary controlling factor of *NEE* at daily to monthly timescales in the studied ecosystem. Temperature may drive plant phenology (e.g., leafout and senescence) and thus modulate *NEE* at seasonal and annual scales. Besides direct drought effects at monthly or longer timescales, episodic periods of soil water deficit can obscure the transfer of *PAR* variability into *NEE* at scales from multi-days to multi-weeks, probably by affecting plant photosynthetic capacity and canopy leaf area index.

Our findings provide several implications for field studies. We illustrated the usefulness of wavelet analysis as a powerful tool for investigating the variability and controlling factors of ecosystem processes. Wavelet techniques could help design field experiments that aim to identify processes regulating CO_2 fluxes at certain timescales (e.g., those correspond to rain pulses and extreme weather events). For a better understanding of regional or global C cycling, future studies should investigate how WTC patterns (i.e., amplitudes and phases) between CO_2 fluxes and biophysical factors may vary among vegetation types or successional stages, or along environmental gradients (Vargas et al., 2010, 2012). Moreover, WTC is well-suited for detecting time lags and hysteresis between processes at multiple timescales (Vargas et al., 2010; Ouyang et al., 2014). Detailed information on hysteresis is crucial for a more reliable prediction of climate-C cycle feedbacks (Niu et al., 2011; Vargas et al., 2011). Such experimental work could shed light on the mechanisms controlling spatial and temporal variations in CO_2 fluxes. Spectral information on mass and energy exchange also has the potential to guide gap-filling practices (Baldocchi et al., 2001), since good gap-filling procedures should preserve the spectral properties of measured time series.

Modeling efforts should take into account multi-temporal correlations between *NEE* and biophysical factors in order to improve model-data agreement across timescales. Information provided by wavelet analysis can be used in the selection of input variables and parameterization methods at different timescales. By identifying the dominant bands of wavelet power and WTC for *NEE* and its driving factors, it is possible to create simplified, low-dimensional models which preserve the spectral characteristics of measured *NEE* (Stoy et al., 2005, 2013). Wavelet techniques have been applied to identify structural model deficiencies over multiple timescales (Vargas et al., 2010; Stoy et al., 2013). For example, the times and timescales where a model fails can be indicated by high wavelet power for model residuals (Vargas et al., 2010), or by significant WTC between modeled and measured *NEE* (Stoy et al., 2013). We recommend using wavelet techniques as a standard approach for evaluating model performance in future studies. Finally, although this study focused only on CO_2 fluxes, wavelet techniques are equally applicable to other greenhouse gases (e.g., CH_4 and N_2O) (Furon et al., 2008; Hatala et al., 2012; Koebsch et al., 2015) or water vapor fluxes (Ding et al., 2013).

Acknowledgements

This study was jointly funded by the National Natural Science Foundation of China (NSFC, Proj. No. 31670708, 31670710, and 31361130340) and the Fundamental Research Funds for the Central Universities (Proj. No. 2015ZCQ-SB-02). The U.S.–China Carbon Consortium (USCCC) supported this work via helpful discussions and the exchange of ideas. We thank X. W. Yang, S. J. Liu, G. P. Chen, and C. Zhang for their assistance with field measurements and instrument maintenance. Please contact X. Jia (xinjia@bjfu.edu.cn) or T. S. Zha (tianshanzha@bjfu.edu.cn) for accessing the data used in this study.

Appendix A. Supplementary data

Supplementary material related to this article can be found, in the online version, at doi: https://doi.org/10.1016/j.agrformet.2018.05.009.

References

Ahlström, A., Raupach, M.R., Schurgers, G., Smith, B., Arneth, A., Jung, M., Reichstein, M., Canadell, J.G., Friedlingstein, P., Jain, A.K., Kato, E., Poulter, B., Sitch, S., Stocker, B.D., Voivy, N., Wang, Y.P., Wiltshire, A., Zaehle, S., Zeng, N., 2015. The dominant role of semiarid ecosystems in the trend and variability of the land CO_2 sink. Science 348, 895–899.

Baldocchi, D., Falge, E., Wilson, K., 2001. A spectral analysis of biosphere-atmosphere trace gas flux densities and meteorological variables across hour to multi-year time scales. Agric. For. Meteorol. 107, 1–27.

Berg, A., Findell, K., Lintner, B., Giannini, A., Seneviratne, S., van der Hurk, B., Lorenz, R., Pitman, A., Hagemann, S., Meier, A., Cheruy, F., Ducharne, A., Malyshev, S., Milly, P.C.D., 2016. Land-atmosphere feedbacks amplify aridity increase over land under global warming. Nat. Clim. Change 6, 869–874.

Biederman, J.A., Scott, R.L., Bell, T.W., Bowling, D.R., Dore, S., Garatuza-Payan, J., Kolb, T.E., Krishnan, P., Krofcheck, D.J., Litvak, M.E., Maurer, G.E., Meyers, T.P., Oechel, W.C., Papuga, S.A., Ponce-Campos, G.E., Rodriguez, J.C., Smith, W.K., Vargas, R., Watts, C.J., Yepez, E.A., Goulden, M.L., 2017. CO_2 exchange and evapotranspiration across dryland ecosystems of southwestern North America. Global Change Biol. 23, 4204–4221.

Burba, G., 2013. Eddy Covariance Method for Scientific, Industrial, Agricultural and Regulatory Applications. LI-COR Biosciences, Lincoln, USA.
Ding, R., Kang, S., Vargas, R., Zhang, Y., Hao, X., 2013. Multiscale spectral analysis of temporal variability in evapotranspiration over irrigated cropland in an arid region. Agric. Water Manage. 130, 79–89.
Cazelles, B., Chavez, M., Berteaux, D., Ménard, F., Olav Vik, J., Jenouvrier, S., Stenseth, N.C., 2008. Wavelet analysis of ecological time series. Oecologia 156, 287–304.
Chen, X., Duan, Z., 2009. Changes in soil physical and chemical properties during reversal of desertification in Yanchi County of Ningxia Hui autonomous region. China. Environ. Geol. 57, 975–985.
Falge, E., Baldocchi, D., Olson, R., Anthoni, P., Aubinet, M., Bernhofer, C., Burba, G., Ceulemans, R., Clement, R., Dolman, H., Granier, A., Gross, P., Grünwald, T., Hollinger, D., Jensen, N.O., Katul, G., Keronen, P., Kowalski, A., Lai, C.T., Law, B.E., Meyers, T., Moncrieff, J., Moors, E., Munger, J.W., Pilegaard, K., Rannik, Ü., Rebmann, C., Suyker, A., Tenhunen, J., Tu, K., Verma, S., Vesala, T., Wilson, K., Wofsy, S., 2001. Gap-filling strategies for defensive annual sums of net ecosystem exchange. Agric. For. Meteorol. 107, 43–69.
Fu, Y.L., Yu, G.R., Sun, X.M., Li, Y.N., Wen, X.F., Zhang, L.M., Li, Z.Q., Zhao, L., Hao, Y.B., 2006. Depression of net ecosystem CO_2 exchange in semiarid *Leymus chinensis* steppe and alpine shrub. Agric. For. Meteorol. 137, 234–244.
Furon, A.C., Wagner-Riddle, C., Smith, C.R., Warland, J.S., 2008. Wavelet analysis of wintertime and spring thaw CO_2 and N_2O fluxes from agricultural fields. Agric. For. Meteorol. 148, 1305–1317.
Grinsted, A., Moore, J.C., Jevrejeva, S., 2004. Application of the cross wavelet transform and wavelet coherence to geophysical time series. Nonlinear Processes Geophys. 11, 561–566.
Han, G., Luo, Y., Li, D., Xia, J., Xing, Q., Yu, J., 2014. Ecosystem photosynthesis regulates soil respiration on a diurnal scale with a short-term lag in a coastal wetland. Soil Biol. Biochem. 68, 85–94.
Hatala, J.A., Detto, M., Baldocchi, D.D., 2012. Gross ecosystem photosynthesis causes a diurnal pattern in methane emission from rice. Geophys. Res. Lett. 39http://dx.doi.org/10.1029/2012GL051303. L06409.
Hong, J., Kim, J., 2011. Impact of the Asian monsoon climate on ecosystem carbon and water exchanges: a wavelet analysis and its ecosystem modeling implications. Global Change Biol. 17, 1900–1916.
Huang, J., Yu, H., Guan, X., Wang, G., Guo, R., 2016. Accelerated dryland expansion under climate change. Nat. Clim. Change 6, 166–171.
Huang, J., Yu, H., Dai, A., Kang, L., 2017. Drylands face potential threat under 2 °C global warming target. Nat. Clim. Change 7, 417–422.
Huxman, T.E., Cable, J.M., Ignace, D.D., Alex Eilts, J., English, N.B., Weltzin, J., Williams, D.G., 2004. Response of net ecosystem gas exchange to a simulated precipitation pulse in a semiarid grassland: the role of native versus non-native grasses and soil texture. Oecologia 141, 295–305.
Jarvis, P., Rey, A., Petsikos, C., Wingate, L., Reyment, M., Pereira, J., Banza, J., David, J., Miglietta, F., Borghetti, M., Manca, G., Valentini, R., 2007. Drying and wetting of Mediterranean soils stimulates decomposition and carbon dioxide emission: the “Birch effect”. Tree Physiol. 27, 929–940.
Jia, X., Zha, T.S., Wu, B., Zhang, Y.Q., Gong, J.N., Qin, S.G., Chen, G.P., Kellomäki, S., Peltola, H., 2014. Biophysical controls on net ecosystem CO2 exchange over a semiarid shrubland in northwest China. Biogeosciences 11, 4679–4693.
Jia, X., Zha, T., Gong, J., Wang, B., Zhang, Y., Wu, B., Qin, S., Peltola, H., 2016a. Carbon and water exchange over a temperate semiarid shrubland during three years of contrasting precipitation and soil moisture patterns. Agric. For. Meteorol. 228, 120–129.
Jia, X., Zha, T.S., Gong, J.N., Wu, B., Zhang, Y.Q., Qin, S.G., Chen, G.P., Feng, W., Kellomäki, S., Peltola, H., 2016b. Energy partitioning over a semiarid shrubland in northern China. Hydrol. Processes 30, 972–985.
Keenan, T.F., Gray, J., Friedl, M.A., Toomey, M., Bohrer, G., Hollinger, D.Y., Munger, J.W., O’Keefe, J., Schmid, H.P., Wing, I.S., Yang, B., 2014. Net carbon uptake has increased through warming-induced changes in temperate forest phenology. Nat. Clim. Change 4, 598–604.
Koebsch, F., Jurasinski, G., Koch, M., Hofmann, J., Glatzel, S., 2015. Controls for multi-scale temporal variation in ecosystem methane exchange during the growing season of a permanently inundated fen. Agric. For. Meteorol. 204, 94–105.
Laio, F., Porporato, A., Ridolfi, L., Rodriguez-Iturbe, I., 2001. Plants in water-controlled ecosystems: active role in hydrologic processes and response to water stress II. Probabilistic soil moisture dynamics. Adv. Water Resour. 24, 707–723.
Ng, E.K.W., Chan, J.C.L., 2012. Geophysical applications of partial wavelet coherence and multiple wavelet coherence. J. Atmos. Ocean. Technol. 29, 1845–1853.
Niu, S., Luom, Y., Fei, S., Montagnani, L., Bohrer, G., Janssens, I.A., Gielen, B., Rambal, S., Moors, E., Matteucci, G., 2011. Seasonal hysteresis of net ecosystem exchange in response to temperature change: patterns and causes. Global Change Biol. 17, 3102–3114.
Ouyang, Z., Chen, J., Becker, R., Chu, H., Xie, J., Shao, C., John, R., 2014. Disentangling the confounding effects of PAR and air temperature on net ecosystem exchange at multiple time scales. Ecol. Complex. 19, 46–58.
Papale, D., Reichstein, M., Aubinet, M., Canfora, E., Berhofer, C., Kutsch, W., Longdoz, B., Rambal, S., Valentini, R., Vesala, T., Yakir, D., 2006. Towards a standardized processing of net ecosystem exchange measured with eddy covariance technique: algorithms and uncertainty estimation. Biogeosciences 3, 571–583.
Poulter, B., Frank, D., Ciais, P., Myneni, R.B., Andela, N., Bi, J., Beoquet, G., Canadell, J.G., Chevallier, F., Liu, Y.Y., Running, S.W., Sitch, S., van der Werf, G.R., 2014. Contribution of semiarid ecosystems to inter-annual variability of the global carbon cycle. Nature 509, 600–603.
Qin, Z., Ouyang, Y., Su, G., Yu, Q., Li, J., Zhang, J., Wu, Z., 2008. Characterization of CO_2 and water vapor fluxes in a summer maize field with wavelet analysis. Ecol. Inf. 3, 397–409.
Stoy, P.C., katul, G.G., Siqueira, M.B., Juang, J.Y., McCarthy, H.R., Kim, H.S., Christopher Oishi, A., Oren, R., 2005. Variability in net ecosystem exchange from hourly to inter-annual time scales at adjacent pine and hardwood forests: a wavelet analysis. Tree Physiol. 25, 887–902.
Stoy, P.C., Richardson, A.D., Baldocchi, D.D., Katul, G.G., Stanovick, J., Mahecha, M.D., Reichstein, M., Detto, M., Law, B.E., Wohlfahrt, G., Arriga, N., Campos, J., McCaughey, J.H., Montagnani, L., Paw U, K.T., Sevanto, S., Williams, M., 2009. Biosphere-atmosphere exchange of CO_2 in relation to climate: a cross-biome analysis across multiple time scales. Biogeosciences 6, 2297–2312.
Stoy, P.C., Dietze, M.C., Richardson, A.D., Vargas, R., Barr, A.G., Anderson, R.S., Arain, M.A., Baker, I.T., Black, T.A., Chen, J.M., Cook, R.B., Gough, C.M., Grant, R.F., Hollinger, D.Y., Izaurralde, R.C., Kucharik, C.J., Lafleur, P., Law, B.E., Liu, S., Lokupitiya, E., Luo, Y., Munger, J.W., Peng, C., Poulter, B., Price, D.T., Ricciuto, D.M., Sahoo, A.K., Schaefer, K., Schwalm, C.R., Tian, H., Verbeeck, H., Weng, E., 2013. Evaluating the agreement between measurements and models of net ecosystem exchange at different times and timescales using wavelet coherence: an example using data from the North American carbon program site-level interim synthesis. Biogeosciences 10, 6893–6909.
Tang, J., Baldocchi, D.D., Xu, L., 2005. Tree photosynthesis modulates soil respiration on a diurnal time scale. Global Change Biol. 11, 1298–1304.
Terrence, C., Compo, G.P., 1998. A practical guide to wavelet analysis. Bull. Am. Meteorol. Soc. 79, 61–78.
Vargas, R., Detto, M., Baldocchi, D.D., Allen, M.F., 2010. Multiscale analysis of temporal variability of soil CO_2 production as influenced by weather and vegetation. Global Change Biol. 16, 1589–1605.
Vargas, R., Baldocchi, D.D., Bahn, M., Hanson, P.J., Hosman, K.P., Kulmala, L., Pumpanen, J., Yang, B., 2011. On the multi-temporal correlation between photosynthesis and soil CO_2 efflux: reconciling lags and observations. New Phytol. 191, 1006–1017.
Vargas, R., Collins, S.L., Thomey, M.L., Johnson, J.E., Brown, R.F., Natvig, D.O., Friggens, M.T., 2012. Precipitation variability and fire influence the temporal dynamics of soil CO2 efflux in an arid grassland. Global Change Biol. 18, 1401–1411.
Wang, B., Zha, T.S., Jia, X., Wu, B., Zhang, Y.Q., Qin, S.G., 2014. Soil moisture modifies the response of soil respiration to temperature in a desert shrub ecosystem. Biogeosciences 11, 259–268.
Yu, G.R., Zhu, X.J., Fu, Y.F., He, H.L., Wang, Q.F., 2013. Spatial patterns and climate drivers of carbon fluxes in terrestrial ecosystems of China. Glob. Change Biol. 19, 798–810.
Zha, T., Qian, D., Jia, X., Bai, Y., Tian, Y., Bourque, C.P.A., Ma, J., Feng, W., Wu, B., Peltola, H., 2017. Soil moisture control of sap-flow response to biophysical factors in a desert-shrub species, Artemisia ordosica. Biogeosciences 14, 4533–4544.
Zhang, W.L., Chen, S.P., Chen, J., Wei, L., Han, X.G., Lin, G.H., 2007. Biophysical regulations of carbon fluxes of a steppe and a cultivated cropland in semiarid Inner Mongolia. Agric. For. Meteorol. 146, 216–229.